Degradation by brown rot fungi increases the hygroscopicity of heat-treated wood

Tiina Belt [a,*], Michael Altgen [b], Muhammad Awais [c], Martin Nopens [d], Lauri Rautkari [c]

[a] Natural Resources Institute Finland, Production Systems Unit, Viikinkaari 9, 00790, Helsinki, Finland
[b] Norwegian Institute of Bioeconomy Research, Department of Wood Technology, P.O. Box 115, 1431, Ås, Norway
[c] Aalto University, School of Chemical Engineering, Department of Bioproducts and Biosystems, P.O. Box 16300, 00076, Aalto, Finland
[d] Thuenen Institute of Wood Research, Leuschnerstrasse 91C, 21031, Hamburg, Germany

ABSTRACT

Heat treatment increases the decay resistance of wood by decreasing its hygroscopicity, but the wood material remains degradable by fungi. This study investigated the degradation of heat-treated wood by brown rot fungi, with the aim of identifying fungal-induced hygroscopicity changes that facilitate degradation. Scots pine sapwood samples were modified under superheated steam at 200 and 230 °C and then exposed to *Coniophora puteana* and *Rhodonia placenta* in a stacked-sample decay test to produce samples in different stages of decay. Sorption isotherms were measured starting in desorption from the undried, decaying state to investigate their hygroscopic properties. Although there were substantial differences in degradative ability between the two fungi, the results revealed that decay by both species increased the hygroscopicity of wood in the decaying state, particularly at high relative humidity. The effect was stronger in the heat-treated samples, which showed a steep increase in moisture content at low decay mass losses. The reference samples showed decreased hygroscopicity in absorption from the dry state, while the heat-treated samples still showed an increase at low mass losses. Near infrared spectroscopy showed that the early stages of decay were characterised by the degradation of hemicellulose and chemical changes to cellulose and lignin, which may explain the increase in hygroscopicity. The results provide a new perspective on brown rot decay and offer insight into the degradation of heat-treated wood.

1. Introduction

Heat treatment is a wood modification technique that relies on thermal degradation reactions to bring about changes in wood composition and properties. Of the wood cell wall polymers cellulose, hemicellulose and lignin, heat treatment has the strongest effect on the hemicellulose fraction, resulting in depolymerisation as well as dehydration and volatilisation of the resulting sugar units (Tjeerdsma et al., 1998; González-Peña et al., 2009). Lignin is also affected by heat treatment and undergoes cleavage as well as condensation reactions with itself and with carbohydrate degradation products (Tjeerdsma et al., 1998; Nuopponen et al., 2005; González-Peña et al., 2009). Crystalline cellulose is relatively resistant to thermal degradation, while amorphous cellulose shows behaviour similar to hemicellulose (González-Peña et al., 2009).

The degradative changes caused by heat treatment change the hygroscopicity of the wood material (Hill et al., 2021). Wood is hygroscopic because the wood cell wall polymers all contain hydroxyl groups that attract water molecules, causing the absorption of moisture from the surrounding environment until an equilibrium state is achieved. Most of the hydroxyl groups accessible to water are found on the hemicelluloses, and as hemicelluloses are the most thermally labile cell wall polymer, heat treatment causes a reduction in the hygroscopicity of wood and reduces the amount of water that the wood can absorb at any given relative humidity (Hill et al., 2021). However, the reduction in hygroscopicity is not solely dependent on the loss of mass (Altgen et al., 2016, 2020), hemicellulose (Repellin and Guyonnet 2005) or accessible hydroxyl groups (Rautkari et al., 2013; Altgen et al., 2018). When the modification is carried out under dry conditions, heat treatment also causes other changes in the wood cell walls that further contribute to the reduction in hygroscopicity. Several explanations have been offered to explain the reduction in hygroscopicity, but none of them has been able to fully account for the behaviour of heat-treated wood (Hill et al., 2021).

Heat treatment also improves the decay resistance of the wood material. Although the thermal degradation of the most easily digestible polymers in wood (hemicelluloses) can decrease the rate of fungal degradation, it is thought that the primary reason for the improved decay resistance of heat-treated wood is related to reduced hygroscopicity (Thybring 2013; Ringman et al., 2014, 2019; Zelinka et al., 2016). While the reasons for improved durability as a result of reduced moisture content are not fully understood, it is thought that the improvement is due to inhibited or reduced diffusion of fungal degradative agents into the wood cell wall (Thybring 2013; Ringman et al., 2014, 2019; Zelinka et al., 2016).

Although heat treatment improves decay resistance, wood decaying fungi are still able to colonise the modified substrate and degrade it. Heat treatment appears to both delay the onset of wood degradation as measured by mass loss due to decay and reduce its rate after decay has begun (Ringman et al., 2016). It has also been shown that some wood decaying fungi are more efficient in degrading heat-treated wood than others, with the brown rot fungus *Rhodonia placenta* often emerging as the most efficient degrader (Kamdem et al., 2002; Welzbacher and Rapp 2007; Metsä-Kortelainen and Viitanen 2009; Chaouch et al., 2013). The eventual degradation of heat-treated wood and the differences in degradative ability between fungi suggest that the fungal degradative process may involve modification of the heat-treated wood that make it more amendable to further fungal degradation. As the decay resistance of heat-treated wood is primarily due to its reduced moisture content, it is possible that the modifications induced by fungal degradation counteract the changes caused by heat treatment and render the material more hygroscopic. Sorption isotherm measurements on brown rotted wood have indicated a reduction in hygroscopicity with increasing decay (Anagnost and Smith 1997; Chauhan and Nagaveni 2009; Brischke et al., 2019), but these measurements were conducted after the decaying material had been dried, which means that the moisture behaviour of the wood was not captured in its decaying state. No measurements have been conducted on decayed heat-treated wood. Our hypothesis is that fungal decay increases hygroscopicity in the undried decaying state and that it at least partially eliminates the moisture exclusion effect caused by heat-treatment.

2. Materials and methods

2.1. Wood sample preparation

Defect-free wood blocks sized 8 mm × 8 mm × 12 mm (orientation longitudinal × tangential × radial) were prepared from commercial kiln-dried boards of Scots pine (*Pinus sylvestris*) sapwood obtained from south-east Finland. The wood species was identified based on the anatomical features described by Richter et al. (2004). The blocks were dried at 105 °C for 24 h to determine their initial dry mass (precision 0.0001 g, average initial mass 0.4005 g). Heat treatments were performed in an oven (Air-o-steam Touchline, Electrolux) under superheated steam at atmospheric pressure. The samples were first held at 105 °C for 30 min in the absence of steam, after which steam injection was started and the temperature increased stepwise every 15 min by 15 °C until reaching the treatment temperature. The treatment temperature was held for 3 h, after which the heating was turned off and the temperature allowed to decrease to <100 °C. One set of samples (N = 84) was treated at 200 °C, one at 230 °C, and one was left untreated to act as reference. After heat treatment the samples were vacuum impregnated with deionized water and leached for two weeks with frequent water changes (every 1–3 days) to remove water-soluble degradation products. The leached samples were dried at room temperature for 24 h and then at 105 °C for another 24 h to determine their modified dry mass and mass loss due to treatment. The untreated samples were subjected to the same leaching and drying procedure as the treated samples. Before the decay test the samples were sterilised by ionising radiation (25–50 kGy dose) and then conditioned at 85% RH at room temperature over a saturated solution of KCl for 8 weeks.
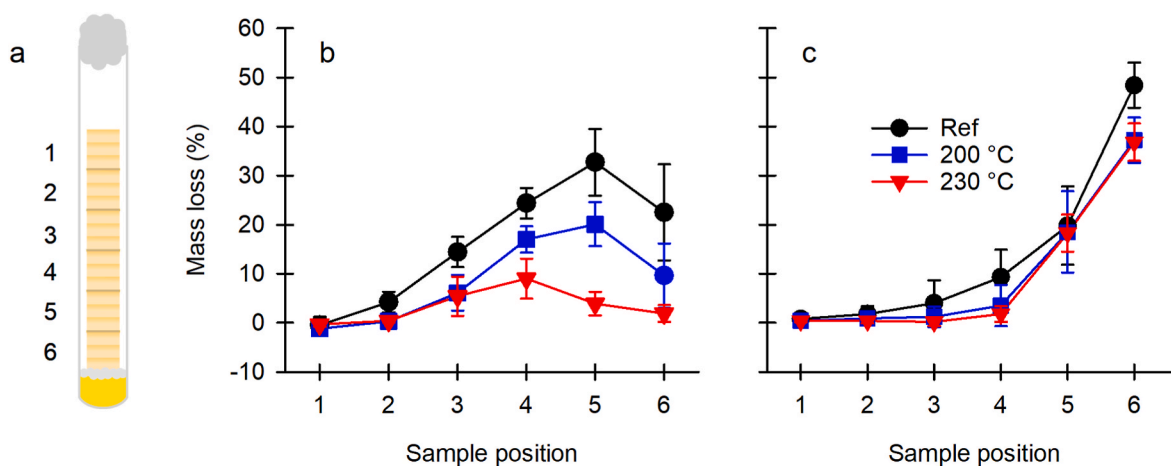
2.2. Decay test

The decay test was performed in 16-mm-diameter glass test tubes using a similar setup as in Belt et al. (2022). The test tubes contained 4 ml of 2% malt extract agar and were inoculated with a plug of mycelium excised from stock cultures of *Coniophora puteana* (strain BAM Ebw. 15) and *Rhodonia placenta* (strain BAM 113) maintained on 2% malt extract agar plates. A piece of plastic netting was placed over the mycelial plug, followed by six wood samples per tube stacked on top of each other (see Fig. 1a). Seven replicate tubes were prepared per sample type and fungus. The tubes were plugged with cotton wool and then incubated at 85% RH (saturated solution of KCl) and room temperature for 15–33 weeks in an area with limited light exposure. All seven replicate tubes corresponding to one wood-fungus combination were removed from the decay test when the visible mycelial front reached the top of the topmost sample in one tube. The samples left untreated, heat-treated at 200 °C and heat-treated at 230 °C were incubated with *C. puteana* for 15, 16 and 26 weeks, respectively, and with *R. placenta* for 33 weeks.

After removal from the decay test, the samples were brushed to remove adhering fungal mycelium and weighed to determine their wet mass. The measured wet masses were used to select one of the seven replicate tubes in each wood-fungus combination for sorption measurements. The samples in these tubes were stored frozen at −20 °C in sealed tubes until analysis, while the samples in the remaining tubes were dried at room temperature for 24 h and then at 105 °C for another 24 h to determine their decayed dry mass and mass loss due to decay. The sorption measurement samples were dried at 105 °C for 24 h after sorption analysis.

2.3. Sorption measurements

The dynamic mass change of the samples during exposure to different relative humidity (RH) steps at a constant temperature of 20 °C was measured in an automated sorption balance (SPSx-1μ-High-Load, ProUmid, Germany). Before the analysis, the samples selected for sorption measurements were soaked in deionized water at room temperature until reaching the water-saturated state. Excess water was removed from the surface before placing the whole samples on aluminium cups in the sample carousel inside the sorption balance. The sample carousel held 24 aluminium cups, of which one was kept empty to correct for a balance drift and one was filled with microcrystalline cellulose as reference material for humidity validation. The remaining cups were used for the simultaneous sorption measurements of all samples degraded by the same decay fungus. The samples were first conditioned at RH steps of 90, 75, 60, 45, 30, 15, and 0% during desorption, before the same RH steps were applied in the reverse order during absorption. The position of each sample was changed regularly by rotating the carousel. The mass of each sample was recorded at 20-min intervals, during which the air flow was stopped. Each RH step was held until the sample mass change was less than 0.01% for all samples, calculated based on the slope of a linear regression line within a 100-min time window that moved forward with each weighing step. The average sample mass within this moving time window was used as reference mass. The step at 0% RH was held for additional 48 h.

After the measurements, the moisture content (MC) at each weighing step was calculated by relating the mass of absorbed water to the dry sample mass, which was determined as the average sample mass within the final hour of the 0% RH step. MC ratios were calculated for each RH step by relating the MC of the samples with the highest decay mass loss to the corresponding MC of the sample with the lowest decay mass loss from the same decay test tube. Finally, the rate of sample MC change was recalculated using the dry sample mass as reference mass and a 3-h regression window. This rate was used as indication if the samples were close to reaching a stable mass at the end of each RH step.

Fig. 1. Sample positions in the stacked-sample decay test (a), and average decay mass losses of the reference and heat-treated (200 °C and 230 °C) samples due to *C. puteana* (b) and *R. placenta* (c) as a function of sample position. The decay test durations for the reference, 200 °C and 230 °C samples were 15, 16 and 26 weeks for *C. puteana* and 33 weeks for *R. placenta*. Error bars are ±SD.

2.4. NIR spectroscopy

The samples used in sorption measurements were analysed by NIR spectroscopy. NIR spectra were acquired in reflectance mode using a Specim SWIR (Specim, Spectral Imaging, Ltd.) short wavelength infrared hyperspectral camera. Images were collected from the radial surfaces of the decayed samples after smoothing the sample surfaces using a rotary microtome. The prepared samples were stored in sealed tubes with silica gel until imaging to prevent the absorption of moisture. The samples to be imaged were placed on a vertical translation stage under the camera, and the height of the stage was adjusted to match each sample surface with the focal plane of the camera. Images were recorded in line scanning mode, with each scan recording 384 pixels and 288 spectral variables over a spectral range of 930–2550 nm at a spectral resolution of 12 nm (full width at half maximum). A calibration reflectance target was scanned along with the samples, resulting in overall image dimensions of 1244 × 384 pixels. The camera was equipped with an OLES macro lens with a field of view of 10 mm, yielding images with a nominal pixel size of ~26 × 26 µm². Two halogen lamps generated polychromatic light, and a HgCdTe detector array with a grating prism monochromator gathered the reflected wavelengths from the exposed surface of the samples.

2.5. Spectral data analysis

The raw NIR images consisted of the imaged sample, the background and the reflectance target. The removal of the background was accomplished by performing principal component analysis (PCA) and applying a threshold to the principal component scores (Bro and Smilde 2014; Amigo et al., 2015). The extracted pixels were subsequently corrected with the recorded spectral reflectance target and the dark current intensities (Mäkelä et al., 2020). The region of interest was selected based on rectangular coordinates originating from the local centre of the sample, resulting in an image with dimensions of 331 × 277 pixels. The images were converted into a two-dimensional array, and an average spectrum was extracted from each image. The acquired average spectrum was then converted into absorbance using the equation A = log10 (1/r), where A represents the estimated absorbance and r represents the unitless reflectance values.

Two separate test sets were prepared for the two fungi, with each set consisting of 18 objects arranged in rows and the wavelengths in columns. The wavelength range was restricted to 1400–2400 nm (179 spectral variables). The test sets underwent pre-processing using the standard normal variate (SNV) method (Barnes et al., 1989), followed by

mean centring. PCA (Bro and Smilde 2014) was conducted separately on each test set. The general PCA model is defined by Equation 1:

$$X = t_1 p_1^T + t_2 p_2^T + \ldots + t_n p_n^T + E_n$$

X denotes the pre-processed test data matrix containing objects spectra, t represents orthogonal scores, p contains orthonormal loading vectors, and E_n represents a residual matrix. The score values were subsequently interpreted with their corresponding loading vectors. Data analysis was performed using a combination of in-house MATLAB (MathWorks, Inc.) scripts and commercial functions from the PLS Toolbox (Eigenvector Research, Inc.).

3. Results

3.1. Mass loss

The heat-treatment of the Scots pine sapwood samples at 200 and 230 °C resulted in average treatment mass losses of 5.9 ± 0.4% and 12.3 ± 0.7%, respectively. The decay mass losses caused by *C. puteana* and *R. placenta* on the treated samples and the untreated references are given in Fig. 1 as a function of sample position in the stacked-sample test. As the objective was to produce a range of decay mass losses in the reference and treated samples, different test durations were used for the different wood-fungus combinations. Fungal colonisation of the samples was used as the end criterion, with each test ending when the visible mycelial front of the fungus had reached the top of the topmost block in one replicate sample stack.

C. puteana colonised the untreated reference samples in 15 weeks, producing a linear increase in decay mass loss from −0.5% to 32.7% from sample position 1 (top) to position 5, followed by a decrease in mass loss at position 6 (bottom). The decrease in mass loss may be due to the presence of nutrient agar residues on the sides of the decay test tubes, which may have allowed the fungus to grow along the agar rather than through the bottommost sample. The samples treated at 200 °C were colonised by *C. puteana* in 16 weeks and reached a decay mass loss of 20.1% at position 5, while the samples treated at 230 °C were colonised more slowly over the course of 26 weeks and reached a maximum decay mass loss of only 9.0%. In the samples treated at 230 °C, maximum mass loss was reached at position 4 rather than position 5. *R. placenta* grew into the samples more slowly than *C. puteana*, taking 33 weeks to colonise the reference as well as the heat-treated samples. The decay mass losses caused by *R. placenta* increased nonlinearly from position 1 to position 6, reaching an average of 48.4% in the reference samples. The decay mass losses of the heat-treated samples were only

slightly lower than those of the reference samples, and there was virtually no difference between the samples treated at 200 °C and 230 °C.

3.2. Sorption measurements

In agreement with previous findings (Ringman et al., 2016), our results showed that heat-treated wood can be colonised and degraded by fungi. To investigate the hygroscopicity changes caused by fungal degradation, we measured the sorption isotherms of the decayed samples starting in desorption from an undried, water-saturated state to capture the hygroscopic properties of the samples in their decaying state, followed by absorption to assess their properties after drying. The isotherms of reference and treated samples with minimum decay mass loss are given in Fig. 2a, while the isotherms of the samples with maximum decay mass loss due to *C. puteana* and *R. placenta* are given in Fig. 2b and c. All sorption isotherms are shown in Fig. S1.

The sorption isotherms of the minimally decayed reference and heat-treated samples showed a clear reduction in hygroscopicity as a result of heat treatment, particularly at high RH. Decay by both *C. puteana* and *R. placenta* on the other hand resulted in increased hygroscopicity. To clearly show the changes in the sorption isotherms from the minimally degraded samples to those with maximum decay mass loss, MC ratios were calculated by dividing the MC of the sample with maximum mass loss by the MC of the sample with minimum mass loss (Fig. 2d–f). The ratios show that in the untreated reference (Fig. 2d), decay resulted in an increase in MC at 90% RH in desorption from the saturated, undried state and a slight decrease in MC over the entire hygroscopic range in absorption from the dry state. In the samples heat-treated at 200 °C (Figs. 2e) and 230 °C (Fig. 2f), the desorption MCs showed an increase over the entire hygroscopic range but particularly at 90% RH. The increase was stronger in the samples treated at 230 °C and in the samples degraded by *R. placenta*. The samples treated at 230 °C also showed a clear increase in MC in absorption. Although the RH steps used in

sorption measurements were not held until constant sample mass, the mass changes measured at the end of each step were less than $|3|$ µg g^{-1} min^{-1} (see Fig. S2), in line with stability criterion recommended by Glass et al. (2018). This means that the samples were close to reaching equilibrium and that the differences in MC seen between the decayed and undecayed samples were due to differences in MC and not to differences in sorption rate.

To gain more insight into the hygroscopicity changes caused by decay, the MCs of the samples at 90% RH in both desorption and absorption were plotted against decay mass loss caused by *C. puteana* and *R. placenta* (Fig. 3). In the untreated reference samples the MC in desorption increased over the entire measured mass loss range, while in absorption the MC decreased slightly as a function of mass loss. The heat-treated samples showed a strong increase in MC in desorption at low decay mass losses (<5%), followed by a more gradual increase in MC upon further mass loss similar to the increase seen in the reference samples. Unlike the reference samples, however, the increase in MC at low mass losses was also visible in absorption, and no decrease in absorption MC as a function of mass loss was seen in the heat-treated samples. Finally, despite the differences in their ability to degrade heat-treated wood, the two fungi produced similar increases in MC at a given decay mass loss.

3.3. NIR spectroscopy

The SNV transformed and mean-centred average NIR spectra of the samples with minimum and maximum mass loss due to decay are shown in Fig. 4, while the average spectra of all samples used for sorption measurements are given in Fig. S3. Important NIR bands are summarised in Table S1. For both fungi, the samples with minimum decay mass loss revealed substantial spectral differences between the heat-treated and reference samples. All three sample types had a positive band at 1906 nm assigned to hemicellulose (Schwanninger et al., 2011), but its intensity was highest in the reference samples, indicating a decrease in
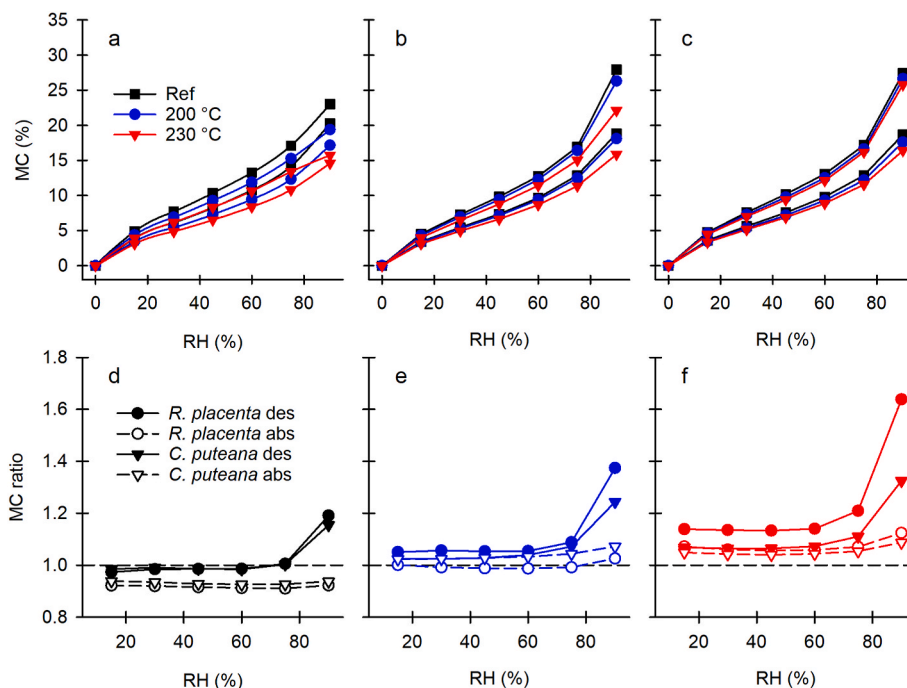
Fig. 2. Sorption isotherms of reference and heat-treated (200 °C and 230 °C) samples with minimum decay mass loss (a) and with maximum decay mass loss due to *C. puteana* (b) and *R. placenta* (c), and moisture content (MC) ratios of reference (d), 200 °C heat-treated (e) and 230 °C heat-treated (f) samples with maximum mass loss due to *C. puteana* and *R. placenta*. MC ratios were calculated by dividing the MC of the sample with maximum decay mass loss by the MC of the corresponding sample with minimum decay mass loss. The decay mass losses of the maximum decay reference, 200 °C and 230 °C samples were 42.8, 22.3 and 12.8% due to *C. puteana* and 49.2, 45.4 and 39.8% due to *R. placenta*.
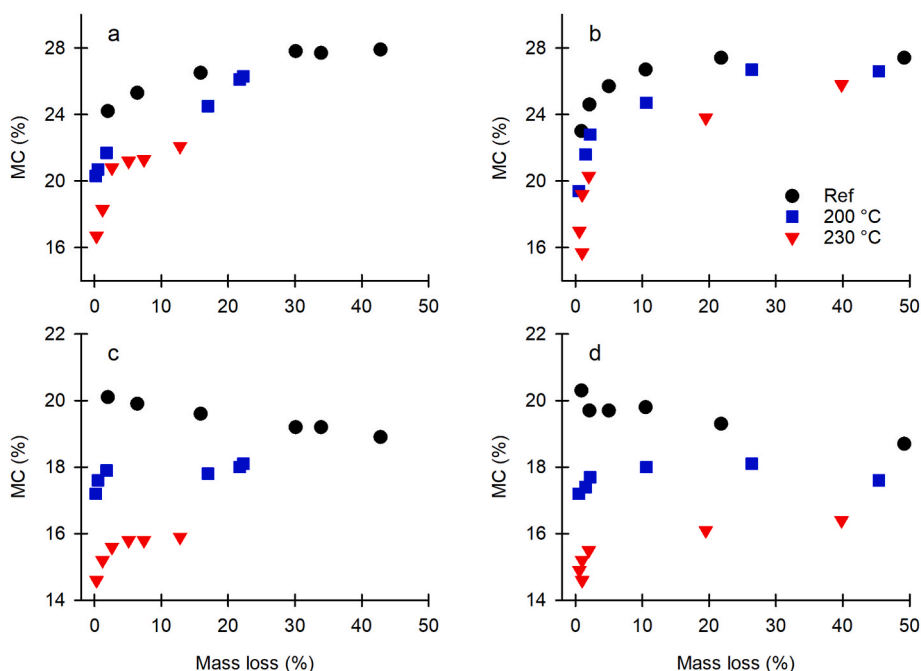
Fig. 3. Moisture contents (MC) of reference and heat-treated (200 °C and 230 °C) samples at 90% RH in desorption from the undried, saturated state (a, b) and in subsequent absorption from the dry state (c, d) as a function of decay mass loss due to *C. puteana* (a, c) and *R. placenta* (b, d).
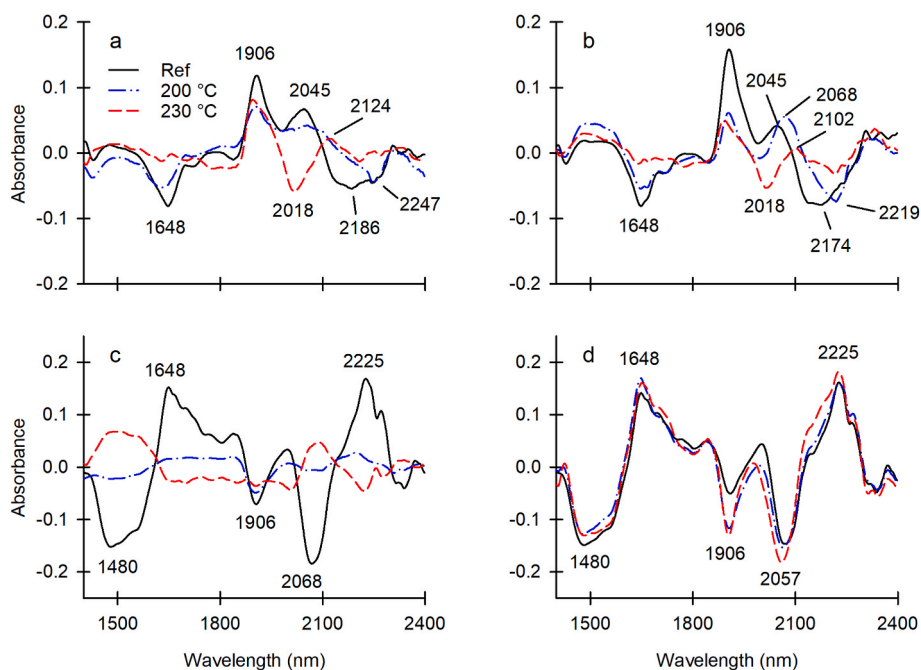
Fig. 4. SNV transformed and mean-centred average NIR spectra of reference and heat-treated (200 °C and 230 °C) samples with minimum decay mass loss (a, b), and maximum decay mass loss (c, d) due to *C. puteana* (a, b) and *R. placenta* (c, d). The decay mass losses of the maximum decay reference, 200 °C and 230 °C samples were 42.8, 22.3 and 12.8% due to *C. puteana* and 49.2, 45.4 and 39.8% due to *R. placenta*.

hemicellulose content as a result of heat treatment. All three sample types also had a positive band at 2045–2124 nm. These bands were assigned to cellulose (Schwanninger et al., 2011; Belt et al., 2022), and the changes in their intensity and position are likely to reflect changes in carbohydrate composition and crystallinity due to heat treatment. The average spectra of all three sample types had negative bands at 1648 nm and 2174–2247 nm. The 1648 nm band was assigned to the aromatic C–H stretch of lignin (Schwanninger et al., 2011; Belt et al., 2022), and the increase in its intensity in the heat-treated samples is a reflection of

increased lignin aromatic content. The 2174–2247 nm bands are also likely to be lignin-derived, and the changes in their intensity and position reflect both the increase in lignin content and changes to its composition.

In the most extensively decayed samples, the reference samples degraded by *C. puteana* and *R. placenta* showed positive bands at 1648 nm and 2225 nm and negative bands at 1480, 1906 and 2068 nm. The band at 1648 nm was again assigned to lignin, and while the 2225 nm band could not be conclusively identified based on the literature, it has

been previously found in brown rot degraded pine sapwood in association with other lignin bands and is therefore also likely to be lignin-derived (Belt et al., 2022). The negative bands were assigned to carbohydrates: 1480 nm to semi-crystalline cellulose (Schwanninger et al., 2011), 1906 nm to hemicellulose (Schwanninger et al., 2011), and 2068 nm to cellulose (Schwanninger et al., 2011; Belt et al., 2022). In the *C. puteana* sample set, the average spectra of the decayed heat-treated samples differed substantially from the decayed reference spectrum, presumably due to the low decay mass losses recorded in the treated samples, while in the case of *R. placenta*, the heat-treated and reference samples showed very similar spectral features, suggesting that *R. placenta* decay brings the composition of the heat-treated samples closer to that of the reference.

To identify the most important spectral changes associated with decay, the NIR spectra were analysed by PCA. Given its efficiency in degrading heat-treated wood (Fig. 1), the results on the *R. placenta* sample set are shown in Fig. 5 and discussed below, while the results on the *C. puteana* sample set are given in Fig. S4. In the *R. placenta* data set, PCs 1, 2 and 3 explained 83.8%, 11.0% and 2.9% of the data variation, respectively. The PC1 loading showed positive bands at 1648 nm (lignin) and 2225 nm (lignin) and negative bands at 1480 nm (semi-crystalline cellulose), 1906 nm (hemicellulose) and 2063 nm (cellulose), which means that PC1 effectively separates the samples according to their lignin-carbohydrate ratio. The PC2 loading on the other hand had a strong positive band at 1906 nm (hemicellulose) and negative bands at 1491 nm (cellulose) and 2118 nm. The 2118 nm band was tentatively assigned to cellulose; bands in the region of 2100–2120 nm were previously found to first increase and then decrease over the course of brown rot decay (Belt et al., 2022), in agreement with the assignment to cellulose. The PC2 loading also had a smaller positive band at 2012 nm. The band could not be conclusively assigned, but it has been previously found in association with lignin-derived bands in wood degraded by *R. placenta* (Belt et al., 2022) and may therefore represent brown rot-related changes to lignin. Given the dominance of the

carbohydrate-derived bands in the loading, PC2 can be thought of as primarily separating the samples according to their hemicellulose-to-cellulose ratio. Finally, the PC3 loading had a positive band at 2023 nm and negative bands at 1603, 1895, 2270 and 2331 nm. The band at 2023 nm is likely to be of similar lignin-derived origin as the 2012 nm band in PC2, while the 1603 nm and 2270 nm bands are derived from crystalline cellulose and cellulose or hemicellulose, respectively (Schwanninger et al., 2011). The 1895 nm band could not be conclusively identified but it is likely due to the C=O stretch of lignin or hemicellulose (Schwanninger et al., 2011; Popescu and Popescu 2013). Bands at similar wavelengths have been previously detected in brown rotted wood where they first decreased and then increased over the course of decay (Belt et al., 2022), suggesting that they may be derived from lignin. PC3 therefore separates the samples according to modifications to lignin and cellulose.

The PC1 vs. PC2 score plot showed that PC2 in particular provided effective separation of the samples according to treatment. The PC2 scores were the highest in the reference samples and the lowest in the samples heat-treated at 230 °C, indicating a decrease in hemicellulose-to-cellulose ratio with treatment. Despite these differences in initial composition, all three sample types showed similar changes in their PC1 and PC2 scores with increasing decay (=position in the decay test tube). The earliest stages of decay (positions 1–3) were characterised by a decrease in PC2 scores with little change in PC1 scores, indicating that the samples underwent a decrease in hemicellulose content with little change to overall lignin-to-carbohydrate ratio. The presence of the 2012 nm band in the PC2 loading tentatively assigned to lignin suggests that the initial decrease in hemicellulose content may be accompanied by chemical changes to lignin. From position 4 onwards the PC1 scores increased, revealing extensive carbohydrate degradation and an increase in residual lignin content. The PC2 scores increased as well, suggesting an increase in hemicellulose-to-cellulose ratio as a result of cellulose degradation.

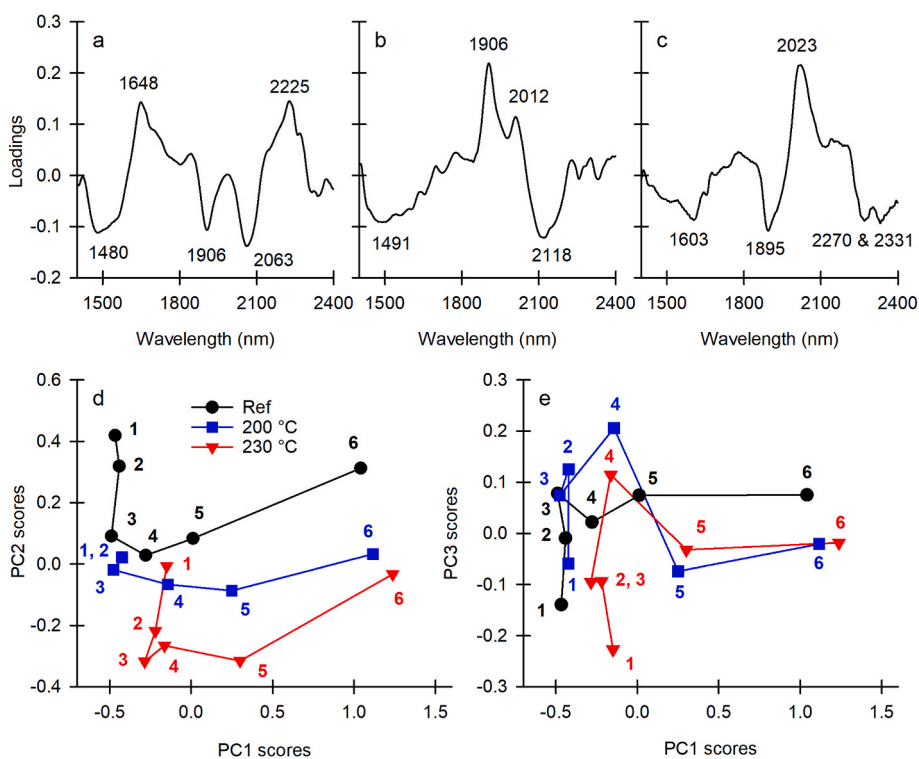The PC1 vs. PC3 score plot also revealed similar spectral changes for

Fig. 5. Principal component analysis of average NIR spectra from reference and heat-treated (200 °C and 230 °C) samples degraded by *R. placenta*. Loadings of principal component (PC) 1 (a), 2 (b) and 3 (c), and score plots of PC1 vs. PC2 (d) and PC1 vs. PC3 (e). The numbers on the score plots refer to the positions of the samples in the decay test tubes.

all three sample types with increasing decay. The PC3 scores increased in the early stages of decay (positions 1–3 in reference samples and positions 1–4 in heat-treated samples), then decreased and finally stabilised in the late stages of decay. The initial increase and subsequent decrease in PC3 scores were stronger in the heat-treated samples than the references. The tentative assignment of the 2023 nm band to lignin suggests that the early stages of decay involve an increase in an unspecified functionality in lignin, followed by a decrease in more advanced decay. The 1895 nm band tentatively assigned to lignin C=O suggests changes in carbonyl functionality; unlike the 2023 nm band, this band first decreased and then increased in more advanced decay. The lignin-related changes were accompanied by a decrease in cellulose-derived bands at 1603 nm and 2270 nm in early stages of decay, followed by an increase in later stages. The 1603 nm band is derived from crystalline cellulose (Schwanninger et al., 2011), which means that the changes may indicate a decrease in cellulose crystallinity in the early decay stages.

4. Discussion

The mass losses recorded after the decay test (Fig. 1) revealed notable differences in degradative ability between the two fungi. The *C. puteana* results demonstrated the durability-enhancing effect of heat treatment; treatment at 230 °C was particularly effective, resulting in greatly increased colonisation time and reduced decay mass loss at full colonisation. Previous studies have produced similar results, with treatment mass loss in the range of 12–15% emerging as a threshold for substantially increased decay resistance (Šušteršic et al., 2010; Chaouch et al., 2010, 2013; Mohareb et al., 2012; Altgen et al., 2020). Unlike *C. puteana*, *R. placenta* colonised all the samples at equal rates, and there was little difference in the decay mass losses recorded for reference and heat-treated samples. Many previous studies have also shown *R. placenta* to be an effective degrader of heat-treated wood, commonly producing high mass losses compared to other wood decaying basidiomycetes (Kamdem et al., 2002; Welzbacher and Rapp 2007; Metsä-Kortelainen and Viitanen 2009; Chaouch et al., 2013). The degradative efficiency of *R. placenta* usually decreases at 10–15% treatment mass loss (Šušteršic et al., 2010; Chaouch et al., 2010, 2013; Mohareb et al., 2012; Altgen et al., 2020), but no decrease was seen in this experiment.

The sorption isotherm measurements (Figs. 2 and 3) revealed a reduction in hygroscopicity due to heat treatment, in agreement with previous studies on wood heat-treated under superheated steam (Olek et al., 2013; Altgen et al., 2016; Lillqvist et al., 2019; Čermák et al., 2022). The decrease was particularly strong at high RH, which is thought to be due to heat-induced changes that increase the stiffness of the cell wall matrix, resulting in increased resistance to cell wall expansion and thus reduced MC (Altgen et al., 2016). A decrease in MC at high RH has also been seen in wood modified using cross-linking agents (Himmel and Mai 2015; Awais et al., 2022).

The sorption results on the decayed samples on the other hand revealed an increase in hygroscopicity in desorption from the undried state, in contrast to results obtained from previous experiments on dried samples (Anagnost and Smith 1997; Chauhan and Nagaveni 2009; Brischke et al., 2019). The increase was particularly strong at low decay mass losses in the heat-treated samples (Fig. 3). In contrast to the reference samples, the heat-treated samples also showed an increase in MC at low mass losses in absorption from the dry state. Our results therefore showed for the first time that the hygroscopicity of wood actually increased as a result of brown rot decay when the measurements were performed before drying, confirming our hypothesis that brown rot increases the hygroscopicity of wood in the wet, decaying state. Our results also revealed that brown rot decay caused additional changes in the heat-treated samples that were not seen in the untreated references, confirming our hypothesis that brown rot degradation partially eliminates the moisture exclusion effect caused by heat treatment.

The samples used for sorption measurements were analysed by NIR spectroscopy to obtain information on the chemical changes responsible for the changes in sorption properties. The spectra (Fig. 4) showed extensive chemical changes in the samples as a result of heat treatment and decay and revealed that advanced decay generally brought the composition of the heat-treated samples closer to that of the untreated reference. The PCA results on the *R. placenta* dataset (Fig. 5) suggest that the early stages of decay were characterised by the degradation of hemicellulose and chemical alterations to cellulose and lignin, in agreement with the established mechanisms of brown rot decay. Brown rot fungi are known to utilise hydroxyl radicals generated by a biological Fenton reaction in the early stages (Arantes et al., 2012; Zhang et al., 2016), resulting in oxidative changes to the wood cell wall polymers. Cellulose is rapidly depolymerised (Kleman-Leyer et al., 1992; Monrroy et al., 2011), while lignin is thought to be depolymerised and subsequently repolymerised, resulting in extensive oxidative modifications to the polymer (Yelle et al., 2008, 2011). After oxidative attack the fungi hydrolyse the cell wall carbohydrates into digestible sugars, with hemicellulose consumed at a faster rate than cellulose (Winandy and Morrell 1993; Curling et al., 2002).

The decrease in the ratio of hemicellulose to cellulose (PC2) is likely to reflect the initiation of hydrolytic carbohydrate degradation, at least in the reference samples, where the decay mass loss reached 5% at position 3. The chemical changes to cellulose and lignin on the other hand are likely the result of oxidative attack. The presence of the 1603 nm band in the PC3 loading suggests that the modifications may include the degradation of crystalline cellulose. Previous research into the effects of brown rot on cellulose crystallinity have revealed an initial increase followed by a decrease over the course of decay (Howell et al., 2009; Zhu et al., 2022), although some studies found a decrease or no change throughout the decay process (Monrroy et al., 2011). The initial increase in crystallinity is thought to be due to the preferential degradation of amorphous polysaccharides, resulting in an increased proportion of crystalline material. However, it is possible that crystalline cellulose is also degraded in early decay as a result of radical attack, just at a lower rate than amorphous components. The degradation of crystalline cellulose would be expected to increase hygroscopicity as OH groups in the tightly packed crystallites become accessible for interaction with water.

The chemical changes to lignin suggested by PC2 and PC3 are tentative and could not be conclusively assigned. However, similar spectral changes have been previously detected by NIR imaging in wood degraded by *R. placenta*: a band at 1894 nm was found to decrease in early decay and then increase in later stages, while a band at 2012 nm was found to increase along with other lignin-derived bands in the latewood regions of the samples (Belt et al., 2022). Brown rot decay is known to cause lignin demethylation and the degradation of inter-unit linkages, resulting in the creation of new functional groups with carbonyl and hydroxyl functionality (Yelle et al., 2008, 2011). The PC3 scores likely reflect these changes. It has been thought that the purpose of the oxidative lignin modification is to open up the wood structure to allow the fungal hydrolytic enzymes to penetrate the wood cell wall (Arantes et al., 2012), but recent studies have indicated that radical attack may instead liberate soluble carbohydrate fragments that diffuse into the cell lumen where they are hydrolysed by the fungal enzymes (Goodell et al., 2017; Zhu et al., 2022). Although the purpose lignin modification and its effects of on the properties of the wood material remain poorly understood, the new functional groups added to the polymer can be expected to increase its hygroscopicity.

The chemical changes revealed by PCA suggest that brown rot decay may increase the hygroscopicity of the wood cell wall polymers. However, the NIR spectra were collected from the samples after drying, which means that the spectra do not represent the samples in their decaying state. Differences in hygroscopicity were seen between the desorption and absorption measurements (Figs. 2 and 3), which suggests the involvement of drying-induced structural rearrangements. Drying-related changes have been documented in untreated wood (Thybring et al., 2017; Penttilä et al., 2020; Paajanen et al., 2022), but they are

even more prominent in hot water extracted wood (Kyyrö et al., 2021), where hemicelluloses have been removed from the cell wall by the treatment. Hot water extraction and decay likely have similar effects: the removal of material creates space in the cell wall that can accommodate water but then collapses upon drying. It is likely that the increased hygroscopicity of the decayed samples in desorption is due both to an increase in cell wall space able to accommodate water and to chemical changes that increase hygroscopicity of the cell wall polymers.

Our results have important implications for the use of heat-treated wood since they indicate that wood decaying fungi can partially eliminate the durability-enhancing moisture exclusion effect provided by the treatment. Heat-treated wood is used in many outdoors applications due to its increased decay resistance, but our results suggest that the resistance will persist only as long as fungal activity is prevented. Heat-treated wood usually performs well in applications without permanent wetting (such as cladding and decking), presumably because its moisture exclusion effect keeps the wood sufficiently dry over extended periods (Welzbacher and Rapp 2007; Humar et al., 2019). However, heat-treated wood shows little resistance in ground-contact where the wetting is permanent (Welzbacher and Rapp 2007), which may be explained by the elimination of decay resistance by fungal activity.

5. Conclusions

Sorption measurements confirmed our hypothesis that brown rot decay increases the hygroscopicity of wood in the undried, decaying state and that brown rot fungi are able to partially eliminate the durability-enhancing moisture exclusion effect of heat-treatment.

Author contributions

Tiina Belt: Conceptualization; Funding acquisition; Investigation; Methodology; Resources; Visualization; Writing - original draft; Writing - review & editing. **Michael Altgen**: Formal analysis; Methodology; Writing - review & editing. **Muhammad Awais**: Formal analysis; Software; Writing - review & editing. **Martin Nopens**: Methodology; Writing - review & editing. **Lauri Rautkari**: Funding acquisition; Writing - review & editing.

Declaration of competing interest

The authors declare that they have no known competing financial interests or personal relationships that could have appeared to influence the work reported in this paper.

Data availability

The datasets presented in this study can be found online at: 10.5281/zenodo.7980675.

Acknowledgments

Appendix A. Supplementary data

Supplementary data to this article can be found online at https://doi.org/10.1016/j.ibiod.2023.105690.

References

Altgen, M., Hofmann, T., Militz, H., 2016. Wood moisture content during the thermal modification process affects the improvement in hygroscopicity of Scots pine sapwood. Wood Sci. Technol. 50, 1181–1195. https://doi.org/10.1007/s00226-016-0845-x.

Altgen, M., Kyyrö, S., Paajanen, O., Rautkari, L., 2020. Resistance of thermally modified and pressurized hot water extracted Scots pine sapwood against decay by the brown-rot fungus Rhodonia placenta. Eur. J. Wood Prod. 78, 161–171. https://doi.org/10.1007/s00107-019-01482-z.

Altgen, M., Willems, W., Hosseinpourpia, R., Rautkari, L., 2018. Hydroxyl accessibility and dimensional changes of Scots pine sapwood affected by alterations in the cell wall ultrastructure during heat-treatment. Polym. Degrad. Stabil. 152, 244–252. https://doi.org/10.1016/j.polymdegradstab.2018.05.005.

Amigo, J.M., Babamoradi, H., Elcoroaristizabal, S., 2015. Hyperspectral image analysis. A tutorial. Anal. Chim. Acta 896, 34–51. https://doi.org/10.1016/j.aca.2015.09.030.

Anagnost, S.E., Smith, W.B., 1997. Hygroscopicity of decayed wood: implications for weight loss determinations. Wood Fiber Sci. 299–305.

Arantes, V., Jellison, J., Goodell, B., 2012. Peculiarities of brown-rot fungi and biochemical Fenton reaction with regard to their potential as a model for bioprocessing biomass. Appl. Microbiol. Biotechnol. 94, 323–338. https://doi.org/10.1007/s00253-012-3954-y.

Awais, M., Altgen, M., Belt, T., et al., 2022. Wood–water relations affected by anhydride and formaldehyde modification of wood. ACS Omega 7, 42199–42207. https://doi.org/10.1021/acsomega.2c04974.

Barnes, R.J., Dhanoa, M.S., Lister, S.J., 1989. Standard normal variate transformation and de-trending of near-infrared diffuse reflectance spectra. Appl. Spectrosc. 43, 772–777. https://doi.org/10.1366/0003702894202201.

Belt, T., Awais, M., Mäkelä, M., 2022. Chemical characterization and visualization of progressive Brown rot decay of wood by near infrared imaging and multivariate analysis. Front. Plant Sci. 13, 940745 https://doi.org/10.3389/fpls.2022.940745.

Brischke, C., Stricker, S., Meyer-Veltrup, L., Emmerich, L., 2019. Changes in sorption and electrical properties of wood caused by fungal decay. Holzforschung 73, 445–455. https://doi.org/10.1515/hf-2018-0171.

Bro, R., Smilde, A.K., 2014. Principal component analysis. Anal. Methods 6, 2812–2831. https://doi.org/10.1039/C3AY41907J.

Čermák, P., Baar, J., Dömény, J., et al., 2022. Wood-water interactions of thermally modified, acetylated and melamine formaldehyde resin impregnated beech wood. Holzforschung. https://doi.org/10.1515/hf-2021-0164.

Chaouch, M., Dumarçay, S., Pétrissans, A., et al., 2013. Effect of heat treatment intensity on some conferred properties of different European softwood and hardwood species. Wood Sci. Technol. 47, 663–673. https://doi.org/10.1007/s00226-013-0533-z.

Chaouch, M., Pétrissans, M., Pétrissans, A., Gérardin, P., 2010. Use of wood elemental composition to predict heat treatment intensity and decay resistance of different softwood and hardwood species. Polym. Degrad. Stabil. 95, 2255–2259. https://doi.org/10.1016/j.polymdegradstab.2010.09.010.

Chauhan, S.S., Nagaveni, H.C., 2009. Moisture adsorption behaviour of decayed rubber wood. J. Inst. Wood Sci. 19, 1–6. https://doi.org/10.1179/002032009X12536100261953.

Curling, S.F., Clausen, C.A., Winandy, J.E., 2002. Relationships between mechanical properties, weight loss, and chemical composition of wood during incipient brown-rot decay. For. Prod. J. 52, 6.

Glass, S.V., Boardman, C.R., Thybring, E.E., Zelinka, S.L., 2018. Quantifying and reducing errors in equilibrium moisture content measurements with dynamic vapor sorption (DVS) experiments. Wood Sci. Technol. 52, 909–927. https://doi.org/10.1007/s00226-018-1007-0.

González-Peña, M.M., Curling, S.F., Hale, M.D.C., 2009. On the effect of heat on the chemical composition and dimensions of thermally-modified wood. Polym. Degrad. Stabil. 94, 2184–2193. https://doi.org/10.1016/j.polymdegradstab.2009.09.003.

Goodell, B., Zhu, Y., Kim, S., et al., 2017. Modification of the nanostructure of lignocellulose cell walls via a non-enzymatic lignocellulose deconstruction system in brown rot wood-decay fungi. Biotechnol. Biofuels 10, 179. https://doi.org/10.1186/s13068-017-0865-2.

Hill, C., Altgen, M., Rautkari, L., 2021. Thermal modification of wood—a review: chemical changes and hygroscopicity. J. Mater. Sci. 56, 6581–6614. https://doi.org/10.1007/s10853-020-05722-z.

Himmel, S., Mai, C., 2015. Effects of acetylation and formalization on the dynamic water vapor sorption behavior of wood. Holzforschung 69, 633–643. https://doi.org/10.1515/hf-2014-0161.

Howell, C., Steenkjær Hastrup, A.C., Goodell, B., Jellison, J., 2009. Temporal changes in wood crystalline cellulose during degradation by brown rot fungi. Int. Biodeterior. Biodegrad. 63, 414–419. https://doi.org/10.1016/j.ibiod.2008.11.009.

Humar, M., Kržišnik, D., Lesar, B., Brischke, C., 2019. The performance of wood decking after five years of exposure: verification of the combined effect of wetting ability and durability. Forests 10, 903. https://doi.org/10.3390/f10100903.

Kamdem, D.P., Pizzi, A., Jermannaud, A., 2002. Durability of heat-treated wood. Holz Roh- Werkstoff 60, 1–6. https://doi.org/10.1007/s00107-001-0261-1.

Kleman-Leyer, K., Agosin, E., Conner, A.H., Kirk, T.K., 1992. Changes in molecular size distribution of cellulose during attack by white rot and Brown rot fungi. Appl. Environ. Microbiol. 58, 1266–1270. https://doi.org/10.1128/aem.58.4.1266-1270.1992.

Kyyrö, S., Altgen, M., Seppäläinen, H., et al., 2021. Effect of drying on the hydroxyl accessibility and sorption properties of pressurized hot water extracted wood. Wood Sci. Technol. 55, 1203–1220. https://doi.org/10.1007/s00226-021-01307-4.

Lillqvist, K., Källbom, S., Altgen, M., et al., 2019. Water vapour sorption properties of thermally modified and pressurised hot-water-extracted wood powder. Holzforschung 73, 1059–1068. https://doi.org/10.1515/hf-2018-0301.

Mäkelä, M., Geladi, P., Rissanen, M., et al., 2020. Hyperspectral near infrared image calibration and regression. Anal. Chim. Acta 1105, 56–63. https://doi.org/10.1016/j.aca.2020.01.019.

Metsä-Kortelainen, S., Viitanen, H., 2009. Decay resistance of sapwood and heartwood of untreated and thermally modified Scots pine and Norway spruce compared with some other wood species. Wood Mater. Sci. Eng. 4, 105–114. https://doi.org/10.1080/17480270903326140.

Mohareb, A., Sirmah, P., Pétrissans, M., Gérardin, P., 2012. Effect of heat treatment intensity on wood chemical composition and decay durability of Pinus patula. Eur. J. Wood Prod. 70, 519–524. https://doi.org/10.1007/s00107-011-0582-7.

Monroy, M., Ortega, I., Ramírez, M., et al., 2011. Structural change in wood by brown rot fungi and effect on enzymatic hydrolysis. Enzym. Microb. Technol. 49, 472–477. https://doi.org/10.1016/j.enzmictec.2011.08.004.

Nuopponen, M., Vuorinen, T., Jämsä, S., Viitaniemi, P., 2005. Thermal modifications in softwood studied by FT-IR and UV resonance Raman spectroscopies. J. Wood Chem. Technol. 24, 13–26. https://doi.org/10.1081/WCT-120035941.

Olek, W., Majka, J., Ł, Czajkowski, 2013. Sorption isotherms of thermally modified wood. Holzforschung 67, 183–191. https://doi.org/10.1515/hf-2011-0260.

Paajanen, A., Zitting, A., Rautkari, L., et al., 2022. Nanoscale mechanism of moisture-induced swelling in wood microfibril bundles. Nano Lett. 22, 5143–5150. https://doi.org/10.1021/acs.nanolett.2c00822.

Penttilä, P.A., Altgen, M., Carl, N., et al., 2020. Moisture-related changes in the nanostructure of woods studied with X-ray and neutron scattering. Cellulose 27, 71–87. https://doi.org/10.1007/s10570-019-02781-7.

Popescu, C.-M., Popescu, M.-C., 2013. A near infrared spectroscopic study of the structural modifications of lime (Tilia cordata Mill.) wood during hydro-thermal treatment. Spectrochim. Acta Mol. Biomol. Spectrosc. 115, 227–233. https://doi.org/10.1016/j.saa.2013.06.002.

Rautkari, L., Hill, C.A.S., Curling, S., et al., 2013. What is the role of the accessibility of wood hydroxyl groups in controlling moisture content? J. Mater. Sci. 48, 6352–6356. https://doi.org/10.1007/s10853-013-7434-2.

Repellin, V., Guyonnet, R., 2005. Evaluation of heat-treated wood swelling by differential scanning calorimetry in relation to chemical composition. Holzforschung 59, 28–34. https://doi.org/10.1515/HF.2005.005.

Richter, H.G., Grosser, D., Heinz, I., Gasson, P.E., 2004. IAWA list of microscopic features for softwood identification. IAWA J. 25, 1–70. https://doi.org/10.1163/22941932-90000349.

Ringman, R., Beck, G., Pilgård, A., 2019. The importance of moisture for Brown rot degradation of modified wood: a critical discussion. Forests 10, 522. https://doi.org/10.3390/f10060522.

Ringman, R., Pilgård, A., Brischke, C., Richter, K., 2014. Mode of action of brown rot decay resistance in modified wood: a review. Holzforschung 68, 239–246. https://doi.org/10.1515/hf-2013-0057.

Ringman, R., Pilgård, A., Kölle, M., et al., 2016. Effects of thermal modification on Postia placenta wood degradation dynamics: measurements of mass loss, structural

integrity and gene expression. Wood Sci. Technol. 50, 385–397. https://doi.org/10.1007/s00226-015-0791-z.

Schwanninger, M., Rodrigues, J.C., Fackler, K., 2011. A review of band assignments in near infrared spectra of wood and wood components. J. Near Infrared Spectrosc. 19, 287–308. https://doi.org/10.1255/jnirs.955.

Šušteršic, Ž., Mohareb, A., Chaouch, M., et al., 2010. Prediction of the decay resistance of heat treated wood on the basis of its elemental composition. Polym. Degrad. Stabil. 95, 94–97. https://doi.org/10.1016/j.polymdegradstab.2009.10.013.

Thybring, E.E., 2013. The decay resistance of modified wood influenced by moisture exclusion and swelling reduction. Int. Biodeterior. Biodegrad. 82, 87–95. https://doi.org/10.1016/j.ibiod.2013.02.004.

Thybring, E.E., Thygesen, L.G., Burgert, I., 2017. Hydroxyl accessibility in wood cell walls as affected by drying and re-wetting procedures. Cellulose 24, 2375–2384. https://doi.org/10.1007/s10570-017-1278-x.

Tjeerdsma, B.F., Boonstra, M., Pizzi, A., et al., 1998. Characterisation of thermally modified wood: molecular reasons for wood performance improvement. Holz Roh-Werkstoff 56, 149–153. https://doi.org/10.1007/s001070050287.

Welzbacher, C.R., Rapp, A.O., 2007. Durability of thermally modified timber from industrial-scale processes in different use classes: results from laboratory and field tests. Wood Mater. Sci. Eng. 2, 4–14. https://doi.org/10.1080/17480270701267504.

Winandy, J.E., Morrell, J.J., 1993. Relationship between incipient decay, strength, and chemical composition of douglas-fir heartwood. Wood Fiber Sci. 25, 278–288.

Yelle, D.J., Ralph, J., Lu, F., Hammel, K.E., 2008. Evidence for cleavage of lignin by a brown rot basidiomycete. Environ. Microbiol. 10, 1844–1849. https://doi.org/10.1111/j.1462-2920.2008.01605.x.

Yelle, D.J., Wei, D., Ralph, J., Hammel, K.E., 2011. Multidimensional NMR analysis reveals truncated lignin structures in wood decayed by the brown rot basidiomycete Postia placenta. Environ. Microbiol. 13, 1091–1100. https://doi.org/10.1111/j.1462-2920.2010.02417.x.

Zelinka, S.L., Ringman, R., Pilgård, A., et al., 2016. The role of chemical transport in the brown-rot decay resistance of modified wood. Int. Wood Prod. J. 7, 66–70. https://doi.org/10.1080/20426445.2016.1161867.

Zhang, J., Presley, G.N., Hammel, K.E., et al., 2016. Localizing gene regulation reveals a staggered wood decay mechanism for the brown rot fungus Postia placenta. Proc. Natl. Acad. Sci. USA 113, 10968–10973. https://doi.org/10.1073/pnas.1608454113.

Zhu, Y., Li, W., Meng, D., et al., 2022. Non-enzymatic modification of the crystalline structure and chemistry of Masson pine in brown-rot decay. Carbohydr. Polym. 286, 119242 https://doi.org/10.1016/j.carbpol.2022.119242.